Available online at www.sciencedirect.com
ScienceDirect
Nuclear Physics B Proceedings Supplement 00 (2014) 1–3
Nuclear Physics B Proceedings Supplement

Property measurement of the Higgs boson in the $\gamma\gamma$ final state with the ATLAS detector at the LHC

Yanping Huang[a]

[a]Deutsches Elektronen-Synchrotron (DESY), Hamburg and Zeuthen, Germany

Abstract

With pp collision data sample recorded by the ATLAS experiment at the CERN Large Hadron Collider at center-of-mass energies of 7 TeV and 8 TeV, corresponding to an integrated luminosity of 25 fb^{-1}, an improved measurement of the mass of the Higgs boson is derived from a combined fit to the decay channels $H \to \gamma\gamma$ and $H \to ZZ^* \to 4l$ with improved energy-scale calibrations for photons, electrons and muons as well as other analysis improvements. It is $m_H = 125.36 \pm 0.37(\text{stat}) \pm 0.18(\text{syst})$ GeV. Furthermore, measurement of fiducial and differential cross sections are presented in the $H \to \gamma\gamma$ decay channel using only the 8 TeV data sample with a luminosity of 20.3fb^{-1}. The observed spectra are statistically limited but broadly in line with the theoretical expectations.

Keywords: Higgs, Mass, Fiducial Cross Section, Differential Cross Section, $\gamma\gamma$ final state

1. Introduction

In 2012, the ATLAS and CMS collaborations announced a new particle [1, 2] in the search for the Standard Model (SM) Higgs boson [3, 4] at the CERN Large Hadron Collider. With the increasing dataset, the emphasis has shifted to determining the properties of the new particle and testing the consistensy of the standard Model against the data. The Higgs mass is not predicted in the SM, which is important for precise calculations of electroweak observables including the production and decay properties of the Higgs boson, as well as the coupling structure of the SM Higgs boson, etc. Based on the measured Higgs mass, the fiducial and differential cross sections of $H \to \gamma\gamma$ are presented, which allows a diverse range of physical phenomena to be probed.

2. Calibration and Particle Identification (PID) efficiency of photons

The ATLAS experiment is a general purpose particle physics detector with a forward-backward symmetric cylindrical geometry and near 4π coverage in solid angle as described in [5]. The latest major improvement includes energy-scale calibrations and photon PID efficiency measurement. The energy reconstruction of electrons and photons is optimised using multivariate algorithms. After correcting for modifications of the data taking conditions with time, the stability of the LAr calorimeter response is at the level of 0.05% and the residual non-uniformal is at the level of 0.7% or better. The response of the calorimeter layers are equalised in data and simulation, and the longitudinal profile of the electromagnetic showers is exploited to estimate the passive material in front of the calorimeter and re-optimise the detector simulation. After all corrections, the Z resonance is used to set the absolute energy scale. The achieved calibration accuracy for electrons from Z decays is typically 0.05% in most of the detector acceptance, rising to 0.2% in regions with large amounts of passive material; 0.2% to 1% for electrons with a transverse energy of 10 GeV, and on average of 0.3% for photons. The energy scale is verified using $J/\psi \to ee$ and $Z \to ll\gamma(l = e, \mu)$ decays as shown in Fig.1 [6]. The detector resolution is determined with a relative accuracy better than 10% for electrons and photons up to 60 GeV

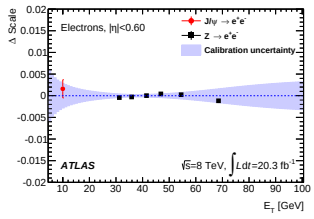

Figure 1: Relative scale difference, Δ Scale, between the measured electron energy scale and the nominal energy scale, as a function of E_T using $J/\psi \to e^+e^-$ events (points with error bars) with $|\eta| < 0.6$. The uncertainty on the nominal energy scale for electrons is shown as the shaded area.

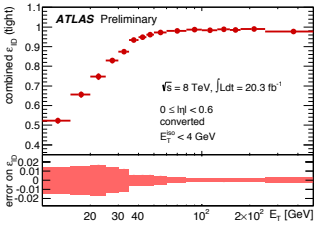

Figure 2: The combination of the data-driven method of ϵ_{ID} for converted photons in the transverse energy of $10GeV < E_T < 500GeV$. The error bar show the statistical and systematic uncertainties from the combination of the measurement in the overlapping E_T regions.

transverse energy, rising to 40% for transverse energies above 500 GeV. There is a combination of three different methods of measurements of $Z \to ll\gamma$ decays, extrapolation from electron in $Z \to ee$ decays, and Matrix methods based on photon purity, the PID uncertainty is at the level of 1% as shown in Fig. 2 [7].

3. Mass measurement

A model-independent approach has been chosen to measure the Higgs boson mass based on fitting of the reconstructed invariant masses spectra of the decay modes $H \to \gamma\gamma$ and $H \to ZZ^* \to 4l$ [6] with a narrow mass peak of a typical experimental resolution of 1.6 GeV to 2 GeV over a smooth background, from which the mass can be extracted without assumptions on the signal production and decay yields. The $H \to \gamma\gamma$ channel profits from an improved calibration of the energy measurements of electron and photon candidates, which results in a sizable reduction of the systematic uncertainties on their energy scales. In the $H \to ZZ^* \to 4l$ channel both the expected statistical uncertainty and the systematic uncertainty on the mass measurement have been reduced with respect to the previous publication. The improvement of the statistical uncertainty arises primarily from the use of a multivariate discriminate

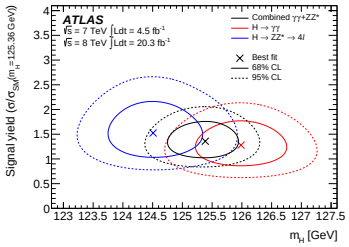

Figure 3: Likelihood contours $-2ln(S, m_H)$ as a function of the normalized signal yield and m_H for the $H \to \gamma\gamma$ and $H \to ZZ^* \to 4l$ channels and their combination, including all systematic uncertainties.

that is designed to increase the separation of the signal from background. The systematic uncertainty reduction comes from both the improved electromagnetic energy calibration and a reduction in the muon momentum scale uncertainty, which was obtained by studying large samples of $Z \to \mu^+\mu^-$ and $J/\psi \to \mu^+\mu^-$ decays.

The combined mass measurement is $m_H = 125.36 \pm 0.37(\text{stat}) \pm 0.18(\text{sys})$ GeV [6], with measured signal strength of $\mu = 1.29 \pm 0.30$ which is set to be free in the fit are shown in Fig.3. No significant correlation between the two fitted variables is observed, confirming the model independence of the mass measurement.

4. Measurement of Fiducial and Differential cross sections

The $H \to \gamma\gamma$ cross section is measured in a fiducial region (baseline) defined by two isolated photons that have absolute pseudorapidity in the interval $|\eta| < 2.37$, with the leading (subleading) photon satisfying $p_T/m_{\gamma\gamma} > 0.35(0.25)$, where p_T is the transverse momentum of the photon and $m_{\gamma\gamma}$ is the diphoton invariant mass. Four additional cross sections contains at least one jet, at least two jets at least three jets and VBF enriched case are studied in ficucial regions, as well as cross-section limits on two VH regions including the single-lepton region and large E_T^{miss} region. The definition is described in [8]. For the differential cross sections, they are measured in the baseline fiducial region for four categories of kinematic variables [8].

- Higgs boson kinematic: $p_T^{\gamma\gamma}$ and $|y_{\gamma\gamma}|$
- Jet activity: N_{jets}, p_T^{j1}, $|y_{j1}|$, p_T^{j2} and H_T
- Spin-CP sensitive variables: $cos\theta^*$ and $|\Delta\phi_{jj}|$
- VBF-sensitive variables: Δy_{jj}, $\Delta\phi_{\gamma\gamma,jj}$

For each fiducial region (or bin of a differential distribution), the signal yield is extracted using a signal plus background fit to the diphoton invariant mass spectrum with the Higgs mass is fixed to 125.36 GeV. The cross sections are determined by correcting these yields for detector inefficiency and resolution, and by accounting for the integrated luminosity of the dataset and is defined by $\sigma_i = \frac{v_i^{sig}}{c_i \int Ldt}$ in a given region.

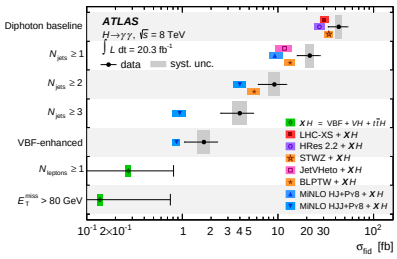

Figure 4: The measured cross sections and cross-section limits for $pp \to H \to \gamma\gamma$ in seven fiducial regions.

Figure 4 shows the comparison between the measured fiducial cross sections and a variety of theoretical predictions. The baseline fiducial cross section is $\sigma_{fid}(pp \to H \to \gamma\gamma) = 43.2 \pm 9.4(\text{stat.})^{+3.2}_{-2.9}(\text{syst.}) \pm 1.2(\text{lumi})\text{fb}$, which is comparable with the LHC-XS prediction [9] of 30.5 ± 3.3fb. The theoretical prediction using HRES [10] for gluon fusion component is slightly smaller than the LHC-XS prediciton for missing electroweak (EW) and threshold resummation correction. STWZ [11] prediction is slightly larger despite the missing EW correction. Although there is a bit of a discrepancy between the measured cross section and theoretical predictions, no significant excess exists. For events containing at least one or two jets, the BLPTW [12] and JetVHeto [13] calculations for the gluon fusion component are in good agreement with the data, while MINLO HJ or MINLO HJJ [14] gives slightly poorer description of the data, same as the case of at least three jets, indicating that the higher order correction included in BLPTW and JetVHeto calculations are important. Finally, in the VBF-enhanced fiducial region, the data are in agreement with MINLO HJJ and POWHEG [14] prediction. The 95% confidence limits on the cross sections in the single-lepton and high-E_T^{miss} fiducial regions are 0.80fb and 0.74fb, respectively.

The bin-by-bin unfolding method is employed in the differential cross section measurement. Figure 5 shows it as a function of $p_T^{\gamma\gamma}$. The data are compared to the SM prediction constructed from the HRES calculation for gluon fusion and the default MC samples for the other

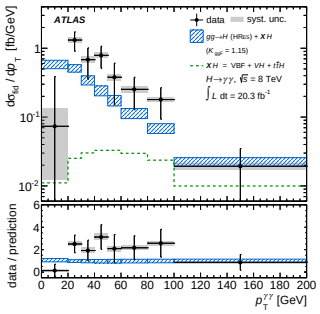

Figure 5: The differential cross section as a function of $p_T^{\gamma\gamma}$.

production mechanisms. The HRES calculation is normalised to the LHC-XS prediction using a $K_{ggF} = 1.15$. The shapes of the distributions are satisfactorily described by the SM prediction, with an overall offset that is consistent with baseline fiducial cross section. Furthermore, the agreement between data and theoretical prediction is quantified with the first and second moment, as well as the χ^2 test. The increased jet activity and harder jet transverse momentum spectra suggest that there is more quark and gluon radiation in the data than in the theoretical prediction. In general, the event generator redictions are in good agreement with the data.

5. Conclusion

With improved energy-scale calibrations for photons, electrons and muons, as well as other analysis improvements, the Higgs mass is measured to be $m_H = 125.36 \pm 0.37(\text{stat}) \pm 0.18(\text{syst})$ GeV. The fiducial and differential cross section of $pp \to H \to \gamma\gamma$ are presented. The observed spectra are statistically limited but broadly in line with the theoretical expectations.

References

[1] ATLAS Collaboration, Phys. Lett. B **716** (2012) 1.
[2] CMS Collaboration, Phys. Lett. B **716** (2012) 30.
[3] F. Englert and R. Brout, Phys. Rev. Lett **13** (1964) 321.
[4] P. Higgs, Phys. Rev. Lett **12** (1964) 132.
[5] ATLAS Collaboration, JINST **3** (2008) S08003.
[6] ATLAS Collaboration, `arXiv:1408.7084 [hep-ex]`.
[7] ATLAS Collaboration, ATLAS-CONF-2014-032.
[8] ATLAS Collaboration, `arXiv:1407.4222 [hep-ex]`.
[9] S. H. et al., `arXiv:1307.1347 [hep-ex]`.
[10] M. Grazzini and H. Sargsyan, JHEP **09** (2013) 129.
[11] I. W. S. et al., `arXiv:1307.1808 [hep-ex]`.
[12] R. B. et al., Phys. Rev. D **89** (2014) 074044.
[13] A. Banfi, Phys. Rev. Lett. **109** (2012) 202001.
[14] K. Hamilton, JHEP **10** (2012) 155.